Project report:
Stability of coaxial skyrmion-vortex configurations due to ferroelectrical effects in ferromagnet-superconductor heterostructures

A. Buskina, S. S. Apostoloff

September 1, 2023

1 Introduction

Mutual influence of magnetism and superconductivity in heterostructures has long history of research. Recently, superconductor–ferromagnet (SF) bilayers hosting topologically nontrivial magnetic configurations have attracted much attention. Skyrmions in SF heterostructures can host Majorana modes and, therefore, serve as a scalable topological quantum computing platform.

In [1] it was predicted that a Néel-type skyrmion and a Pearl vortex interacting via stray fields are repelled from each other to be located at a finite distance. However, Majorana modes are predicted for a coaxial state. In this project we study a way to alter the stability of noncoaxial configuration and to make the skyrmion attract to the center of the vortex.

2 Skyrmion and Pearl vortex

2.1 Model

We consider a thin heterostructure consisting of a thin dielectric ferromagnetic film, a thin superconducting film, and the thin dielectric insulator between them, which suppresses proximity effects.

The free energy of a thin chiral ferromagnetic film interacting with a Pearl vortex is given by

$$F[\mathbf{m}] = d_f \int d^2\mathbf{r} \left(A(\nabla \mathbf{m})^2 + K(1 - m_z^2) + D[m_z \nabla \cdot \mathbf{m} - (\mathbf{m} \cdot \nabla) m_z] - \right. \\ \left. - M_s \mathbf{m} \cdot \mathbf{B}_v \right). \tag{1}$$

Here $\mathbf{m}(\mathbf{r})$ is the unit magnetization vector, M_s is the saturation magnetization, and d_f is the thickness of the ferromagnetic film. Parameters $A > 0$, $K > 0$, and D stand for the exchange, perpendicular anisotropy, and DMI constants, respectively. The z axis is directed perpendicular to the film.

2.2 Derivation of the Euler-Lagrange equation

The magnetization of any radial symmetric configuration can be sought as $\mathbf{m} = \mathbf{e}_r \sin\theta(r) + \mathbf{e}_z \cos\theta(r)$. Substituting this into Eq. (1), we obtain

$$F[\theta(r)] = 2\pi d_f \int dr\, r \left(A \left((\theta')^2 + \frac{\sin^2\theta}{r^2} \right) + K \sin^2\theta + \right. \\ \left. + D \left(\frac{\cos\theta \sin\theta}{r} + \theta' \right) - M_s (B_r \sin\theta + B_z \cos\theta) \right). \tag{2}$$

Minimizing the free energy and rescaling $r \to r/\ell_w$, where $\ell_w = \sqrt{A/K}$ is the domain wall width, we derive the Euler-Lagrange equation,

$$2 \left(\theta'' + \frac{\theta'}{r} \right) - \left(\frac{1}{r^2} + 1 \right) \sin(2\theta) + \frac{4\epsilon \sin^2\theta}{r} + 2\gamma \left(b_z \sin\theta - b_r \cos\theta \right) = 0, \tag{3}$$

where we introduced two dimensionless parameters: the effective strength of the Pearl vortex

$$\gamma = (\ell_w/\lambda)(M_s \phi_0 / 8\pi A)$$

and the DMI strength

$$\epsilon = D/2\sqrt{AK}.$$

The functions $b_r(r)$ and $b_z(r)$ are the rescaled projections of the magnetic field of the Pearl vortex in the ferromagnetic film,

$$B_V = -(\phi_0/4\pi\ell_w\lambda)[b_r(r)\mathbf{e}_r + b_z(r)\mathbf{e}_z].$$

2.3 "No skyrmion" configuration

If condition $\theta(r = 0) = 0$ is assumed, the solution of Eq. (3) describes the magnetization of initially homogeneous ferromagnetic film without a skyrmion in the magnetic field of the Pearl vortex. According to [2], the approximation $b_r \approx b_z \approx 1/r$ can be used and Eq. (3) can be reduced to

$$\theta'' + \frac{\theta'}{r} - \left(\frac{1}{r^2} + 1\right)\theta + \frac{\gamma}{r} = 0. \tag{4}$$

Solving (4) with the second boundary condition $\theta(r = \infty) = 0$, we obtain

$$\theta_\gamma(r) \approx \gamma[K_1(r) - 1/r], \tag{5}$$

where $K_1(x)$ is the modified Bessel function of the second kind.

2.4 Free skyrmion

In this section we try to reproduce well-known results for a free skyrmion described by the solution of

$$2\left(\theta'' + \frac{\theta'}{r}\right) - \left(\frac{1}{r^2} + 1\right)\sin(2\theta) + \frac{4\epsilon \sin^2\theta}{r} = 0 \tag{6}$$

with boundary conditions $\theta(r = 0) = \chi\pi$, where $\chi = \pm 1$ is the chirality of the skyrmion, and $\theta(r = \infty) = 0$. Since Eq. (6) is being solved numerically, both conditions can not be applied directly. So, we can use so-called "shooting" method, replacing them by

$$\theta(r = \xi \ll 1) = \chi\pi \text{ and } \theta'(r = \xi \ll 1) = c,$$

where constant c should be found by the iteration procedure to satisfy condition $\theta(r = \infty) = 0$.

The solution of Eq. (6) can be approximated with high accuracy by 360° domain wall ansatz

$$\theta_{R,\delta}(r) = 2\tan^{-1}\frac{\sinh\left(\frac{R}{\delta}\right)}{\sinh\left(\frac{r}{\delta}\right)}. \tag{7}$$

Having found the numerical solution, we fit it by Eq. (7). The Fig. 1 shows that curves coincide up to $r \approx 15$.

The second way to obtain parameters of the ansatz is to substitute it into Eq. (2) and minimize $F(R, \delta)$. These two approaches can be compared using Fig. 2.

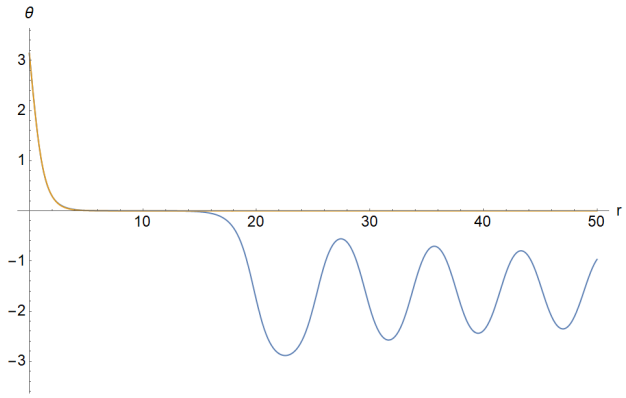

Figure 1: The figure shows solution obtained by "shooting" method for $\epsilon = 0.4$ (blue curve) and its fitting by 360° domain wall ansatz (orange curve).

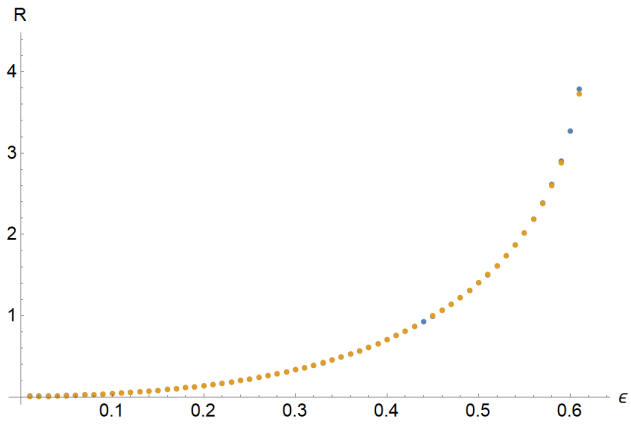

Figure 2: The figure shows $R(\epsilon)$ derived from numerical solutions (blue dots) and from minimizing free energy with the 360° domain wall ansatz (orange dots).

2.5 Skyrmion with vortex

The same methods of analysis, as in the previous section, are applied to the Eq. (3) with $b_z = b_r = 1/r$. In this case the modified 360° domain wall ansatz is given by

$$\begin{aligned}\theta_{R,\delta,\gamma}(r) &= \theta_{R,\delta}(r) + \theta_{\gamma}(r)\cos(\theta_{R,\delta}(r)) \\ &= 2\tan^{-1}\frac{\sinh\left(\frac{R}{\delta}\right)}{\sinh\left(\frac{r}{\delta}\right)} + \gamma\left[K_1(r) - \frac{1}{r}\right]\cos\left[2\tan^{-1}\frac{\sinh\left(\frac{R}{\delta}\right)}{\sinh\left(\frac{r}{\delta}\right)}\right].\end{aligned} \tag{8}$$

We made sure that in this case the solution with negative chirality exists and for some ϵ, γ more than one solution with positive chirality can be found in agreement with [2]. Fig. 3 shows that the modified ansatz gives more precise approximation than well known one.

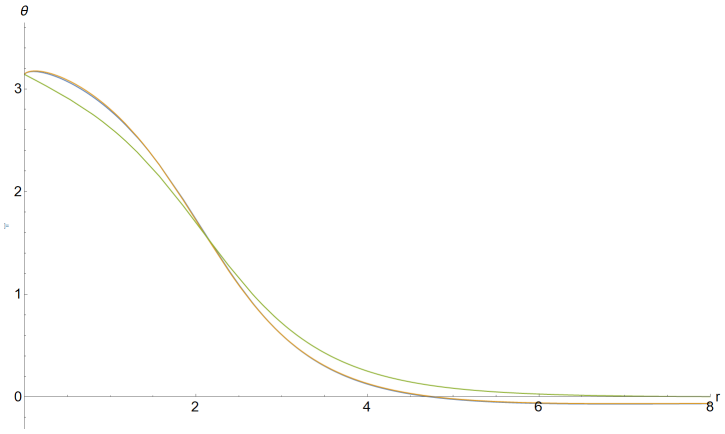

Figure 3: The figure shows one of numerical solutions with positive chirality for $\epsilon = 0.3$, $\gamma = 0.522$ (blue curve), its fitting by 360° domain wall and modified ansatz (green and orange curves respectively).

3 Ferroelectric effects

3.1 Polarization of skyrmion

As it was shown in [3], in inhomogenius ferromagnetic film electric polarization occurs,

$$\mathbf{P} = \alpha\chi_e M_s^2[(\mathbf{m}\cdot\nabla)\mathbf{m} - \mathbf{m}(\nabla\cdot\mathbf{m})] \tag{9}$$

where α is the spin flexoelectric constant, χ_e is the electric susceptibility. Substituting $\mathbf{m} = \mathbf{e}_r \sin\theta(r) + \mathbf{e}_z \cos\theta(r)$ in Eq. (9), we obtain

$$\begin{aligned} P_r &= -\alpha\chi_e M_s^2 \frac{\sin^2\theta}{r}, \\ P_z &= -\alpha\chi_e M_s^2 \left(\theta' + \frac{\sin\theta\cos\theta}{r}\right). \end{aligned} \tag{10}$$

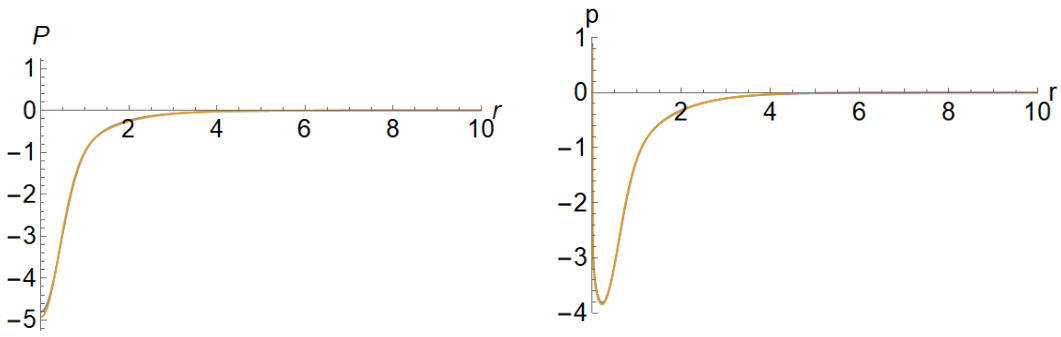

Figure 4: Rescaled projection of the polarization for numerical solution (blue curve) and model fitting (orange curve) for free skyrmion (left panel) and skyrmion with vortex (right panel).

3.2 Extended Euler-Lagrange equation

Interaction of skyrmion with an external elecric field adds

$$\int d^2\mathbf{r} \frac{4\pi\mathbf{P}\cdot\mathbf{E}}{8\pi}$$

to the free energy. In the proximity of the ferromagnetic and superconducting layers the field is perpendicular to the surface, and only components parallel to the z axes are sufficient:

$$\Delta F[\theta] = -\pi d_f \alpha\chi_e M_s^2 \int dr\, r E_z(r) \left(\theta' + \frac{\sin\theta\cos\theta}{r}\right). \tag{11}$$

Note that Eq. (11) looks like DMI term and

$$(\alpha\chi_e M_s^2/2)\sqrt{AK}\left(-2\frac{\sin^2\theta}{r}E_z - \frac{\partial E_z}{\partial r}\right)$$

has to be added to the lhs of Eq. (3),

$$2\left(\theta'' + \frac{\theta'}{r}\right) - \left(\frac{1}{r^2} + 1\right)\sin(2\theta) + \frac{4(\epsilon - \beta e_z)\sin^2\theta}{r} - 2\beta e_z' + 2\gamma\left(b_z \sin\theta - b_r \cos\theta\right) = 0. \tag{12}$$

The function $e_z(r)$ is the rescaled projection of electric field. We also introduced

$$\beta = (\alpha\chi_e M_s^2/2)\sqrt{AK}(E_z/e_z).$$

which can be treated as an effective field strength.

3.3 Point charge field configuration

Since skyrmions have nonzero electric polarization, they can be manipulated, for instance, using a conductive needle with a certain potential. In real experiments the exact configuration of electric field is unknown since it strongly depends on the shape of the tip, which is usually uneven. We attempted to suggest some simple to analyse possible shapes of the needle. In this section we model it with a ball on a thin conductive thread, that is a point charge in the first approximation. Some ideas to specify the model is given in Appendix A.

The charge is placed above thin heterostructure on the height h. So, for large distances between the charge and the superconductor the field near the film is given by

$$E_{q,z}|_{z=+0} = \frac{2qh}{(h^2 + r^2)^{3/2}}. \tag{13}$$

Effective field strength in Eq. (12) for point charge:

$$\beta = qh(\alpha\chi_e M_s^2)\sqrt{AK}.$$

We solved Eq. (12) numerically for $\epsilon > 0$ and $\epsilon < 0$ with nonzero γ and compared these solutions to ones with $\gamma = 0$. Results are given on Fig. 5.

3.4 Ansatz for the extended Euler-Lagrange equation

We assumed that the new ansatz looks like Eq. (8) with $\theta_{\gamma,\beta,h} = \theta_\gamma + \theta_{\beta,h}$, where $\theta_{\gamma,\beta,h}$ is the solution of the corresponding Euler-Lagrange equation for "no skyrmion" configuration in the presence of the point charge. We found

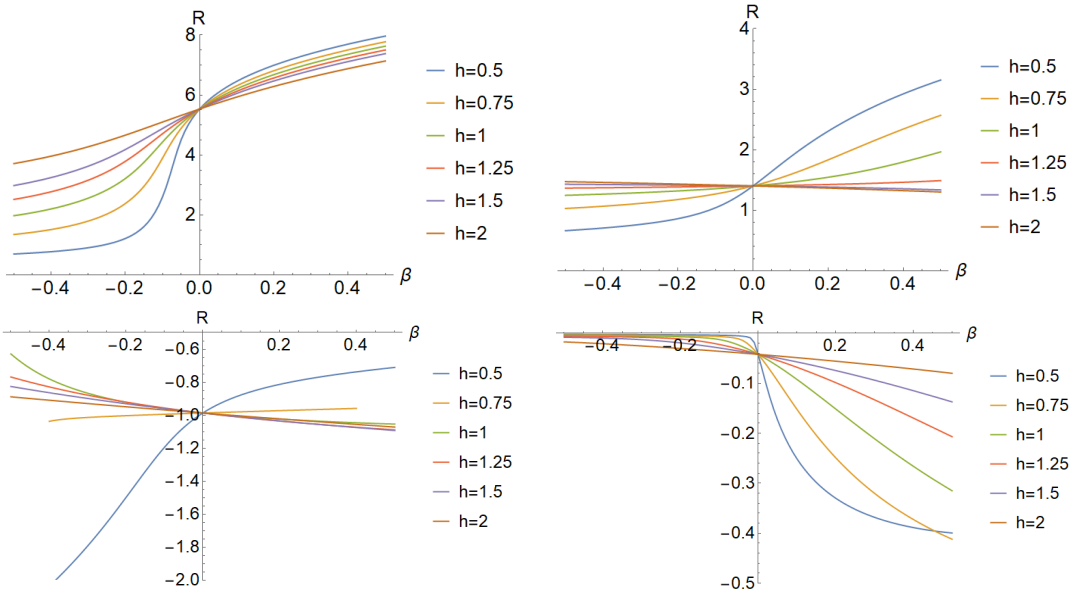

Figure 5: Radius of the skyrmion for different h and (upper panel) $\epsilon = 0.5$, $\gamma = 0.2$ (left), $\gamma = 0$ (right). (Lower panel) $\epsilon = -0.1$, $\gamma = 0.4$ (left), $\gamma = 0$ (right).

that $\theta_{\beta,h} \ll \theta_\gamma$ for small β and fitting the numerical solution of the extended Euler-Lagrange equation by Eq. (8) gives almost the same results for the radius of the skyrmion as the numerical solution of $\theta(r) = \chi\pi/2$.

3.5 Stability of the coaxial configuration

The free energy for slightly shifted configuration is given by

$$\frac{\delta F(a)}{4\pi A d_f} = \int_0^\infty dr\{\gamma r[\delta b_r^a \sin\theta + \delta b_z^a(\cos\theta - 1)] - \beta\delta e_z^a\,(\sin\theta\cos\theta + r\theta')\}, \quad (14)$$

where a is such a small spacing, that the reshaping of the skyrmion in the leading approximation may be neglected. The functions δb_r^a, δb_z^a and δe_z^a mean the difference between the dimensionless r- and z-projections of the vortex field and z-projection of the point charge field averaged by rotation of the system around the center of the skyrmion, i.e., over all possible directions

of the vector a, and fields before shifting.

$$\delta b_r^a = -\frac{\Theta(a-r)}{r}, \quad \delta b_z^a = K\left[\frac{4ar}{(a+r)^2}\right]\frac{2}{\pi(a+r)} - \frac{1}{r} \tag{15}$$

$$\delta e_z^a = \frac{2\sqrt{h^2+(a-r)^2}E\left(-\frac{4ar}{h^2+(-a+r)^2}\right)}{a^4+2a^2(h-r)(h+r)+\left(h^2+r^2\right)^2} + \\ + \frac{2\sqrt{h^2+(a+r)^2}E\left(\frac{4ar}{h^2+(a+r)^2}\right)}{a^4+2a^2(h-r)(h+r)+\left(h^2+r^2\right)^2} - \frac{1}{(r^2+h^2)^{3/2}} \tag{16}$$

Here, $\Theta(z)$ denotes the Heaviside step function, $K(z)$ and $E(z)$ are the complete elliptic integrals of the first and the second kind respectively.

Having numerically integrated Eq. (14), we obtained stability diagram Fig. 6. In the blue region $\delta F(a) - \delta F(0) < 0$, i.e. the coaxial configuration is unstable.

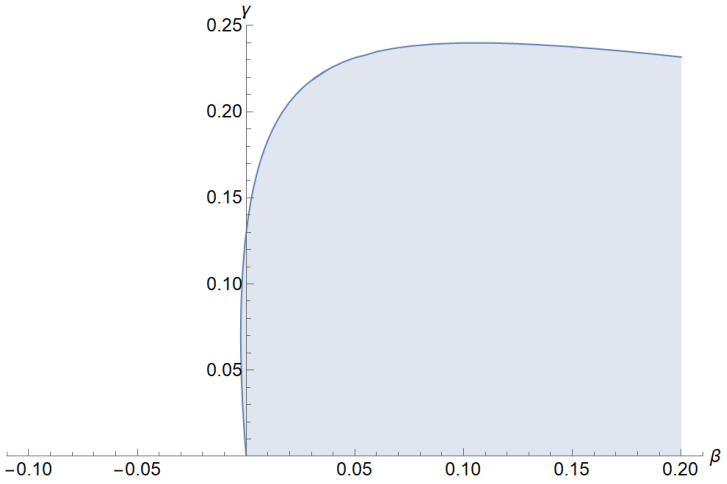

Figure 6: Stability diagram for $\epsilon = 0.4$, $h = 1$. In the blue region the coaxial state is unstable.

A Field of a needle

Since an exact description of a shape of the needle is complicated, we attempted to suggest the simplest model which allows us to express boundary

conditions correctly.

Firstly, we consider an infinite metal plane $z = 0$ and an infinite metal needle coinciding with the z axes for $z_n > h > 0$. After reflecting the needle it is convenient to use prolate spheroidal coordinates

$$\begin{aligned} x &= a\sqrt{(\sigma^2-1)(1-\tau^2)}\cos\varphi \\ y &= a\sqrt{(\sigma^2-1)(1-\tau^2)}\sin\varphi \\ z &= a\sigma\tau \end{aligned} \tag{17}$$

due to a simple formulation of constant potential difference between the plane and the needle condition $\Phi(\tau = \pm 1) = \pm V$. The Laplacian in chosen coordinate system is given by

$$\begin{aligned} \nabla^2\Phi = \frac{1}{a^2(\sigma^2-\tau^2)}\left\{\frac{\partial}{\partial\sigma}\left[\left(\sigma^2-1\right)\frac{\partial\Phi}{\partial\sigma}\right] + \frac{\partial}{\partial\tau}\left[(1-\tau^2)\frac{\partial\Phi}{\partial\tau}\right]\right\} \\ + \frac{1}{a^2(\sigma^2-1)(1-\tau^2)}\frac{\partial^2\Phi}{\partial\varphi^2}. \end{aligned} \tag{18}$$

The last term equals zero due to rotational symmetry. Variables can be separated by substitution $\Phi(\sigma, \tau) = \phi(\sigma)\psi(\tau)$, which leads to

$$\begin{aligned} \left(\sigma^2-1\right)\phi''(\sigma) + 2\sigma\phi'(\sigma) - \lambda\phi(\sigma) = 0 \\ \left(\tau^2-1\right)\psi''(\tau) + 2\tau\psi'(\tau) - \lambda\psi(\tau) = 0 \end{aligned} \tag{19}$$

Anyway, the solution will have logarithmic divergence in proximity of the surface of the needle. One may suggest to solve the problem for the needle of small but finite size. However, in prolate spheroidal coordinates the distance between focal points and the shape of paraboloids are not independent, so the solution obtained for a specific needle shape is correct only for one position.

B Other branches

While solving Eq. (12) for the point charge field we noticed that for small h and large β more than one solution satisfying boundary conditions is present. In the main text We studied solutions corresponding to the minima of free energy, while the rest could correspond to maxima or saddle points. The figure below shows radius dependence on β for 2nd branches. Their stability and conditions for the transition to a stable branch are objects of further research.

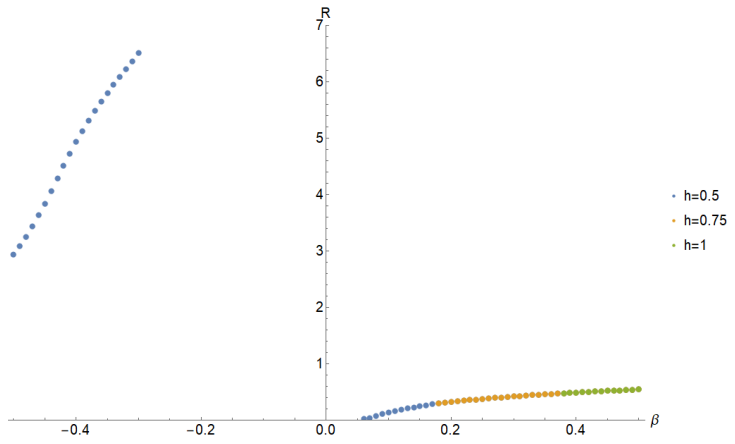

References

[1] E. S. Andriyakhina and I. S. Burmistrov. Interaction of a néel-type skyrmion with a superconducting vortex. *Physical Review B*, 103(17):174519, May 2021.

[2] S. S. Apostoloff, E. S. Andriyakhina, P. A. Vorobyev, Oleg A. Tretiakov, and I. S. Burmistrov. Chirality inversion and radius blowup of a néel-type skyrmion by a pearl vortex. *Phys. Rev. B*, 107:L220409, Jun 2023.

[3] Maxim Mostovoy. Ferroelectricity in spiral magnets. *Phys. Rev. Lett.*, 96:067601, Feb 2006.